Ceramics-Silikáty 64 (4), 371-378 (2020)
www.ceramics-silikaty.cz doi: 10.13168/cs.2020.0011

RECYCLING FLY ASH AND RED MUD TO MANUFACTURE SELF-FOAMING CERAMIC FOAMS

CONGCONG JIANG, XIUZHI ZHANG, DAN WANG, LINA ZHANG, #XIN CHENG

University of Jinan, Jinan 250022, China

#E-mail: ujn_chengxin@163.com

Submitted October 27, 2019; accepted December 20, 2019

Keywords: Ceramic foams, Self-foaming, Fly ash, Red mud

Manufacturing ceramic foams derived from solid waste can not only alleviate hazards to the environment, but also obtain high value-added products. The self-foaming ceramic foams were prepared by recycling fly ash (FA) and red mud (RM) as raw materials. The pore structure, physical and mechanical properties of the sintered foams subjected to different sintering schedules were investigated. The results showed that the ceramic foams performed a self-foaming procedure in the course of sintering, derived from the combustion of the organic materials and/or the decomposition of the carbonates in the studied FA and RM. The sample sintered at 675 °C for 60 min exhibited promising properties, including a bulk density of 331 kg·m^{-3}, a porosity of 83.8 %, a water absorption of 2.91 % and a compressive strength of 1.96 MPa, which has good potential application in the fields of insulation, gardening and lightweight constructions.

INTRODUCTION

Nowadays, the huge volume of industrial wastes has become a key in one of the world's greatest environmental problems, thus, recycling has turned into an important measure to diminish the solid waste landfill and protect the environment. Red mud (RM) comes from the process of alumina extraction from bauxite and fly ash (FA) which is formed as a by-product of coal combustion in power stations have become two major solid wastes. In China, the total production of FA is as high as 650 million tonnes per year [1, 2]. However, the actual recycling utilisation rate of FA is less than 70 % only. Meanwhile, approximately 1 ~ 2 tonnes of RM can be produced with each tonne of alumina production. It is estimated that nearly 30 million tonnes of RM are generated annually in China [3, 4]. Due to the high alkalinity and complexity, the ways of traditional disposal can not only cause severe pollution, but also make the utilisation rate of RM extremely low.

FA contains a large amount of SiO_2 and Al_2O_3, which are the main glass network formers during the sintering and then helps to provide the strength of the resultant ceramic products [5]. For RM, there is a compositional difference between the Bayer process and the sintering process, the most dominant oxides include Al_2O_3, SiO_2, CaO and Fe_2O_3 [4]. Due to the chemical compositions of these two materials being close to that of ceramic raw materials, several researchers have reported on porous ceramics/glasses with different foaming agents using RM and FA as the raw materials. For instance, Chen et al. [6] synthesised a foam ceramic from RM and FA using 5 wt. % sodium silicate ($NaSiO_3$) as the foaming agent, sintered at 900 °C. Guo et al. [3] obtained glass ceramic foams using RM and FA with the addition of calcium carbonate ($CaCO_3$) as the foaming agent fired at 760 ~ 840 °C. Liu et al. [7, 8] manufactured ceramic foams from RM, FA and 18 ~ 20 wt. % lead-zinc mine tailings as the foaming agent at 980 °C. Foam glasses by consuming up to 33.3 ~ 43.3 wt. % FA, adding 0.5 wt. % SiC as the foaming agent and firing at 865 ~ 915 °C were obtained by Li et al. [2]. Chen et al. [9, 10] fabricated foam glasses with a high content (50 ~ 70 wt. %) of FA at the sintering temperature of 800 °C using calcium carbonate ($CaCO_3$) as the foaming agent. These examples have involved the addition of various foaming agents and their dispersion within the raw mixtures. Besides, Luo et al. [11] obtained a new ceramic foam entirely from the pre-treated FA that was evenly coated with a layer of hydroxy-sodalite crystals, revealing that the pre-treated FA underwent a self-foaming reaction during sintering at a temperature of 1200 °C. However, few reports have been discussed on the facile preparation of porous ceramics based on fly ash and red mud as the raw materials without any foaming agent and pre-treatment.

In this paper, ceramic foams were obtained from the studied RM and FA with sodium borate as the flux agent, without any additional foaming agent and pre-treatment. This study aspired to address the pore-forming mechanism, as well as the effect of the sintering temperature and the holding time were discussed in detail.

EXPERIMENTAL

Raw materials

The as-received FA was sampled from a coal-fired power station in Shandong Province, the RM was gathered from an aluminium factory in Jinan. Both the chemical compositions of the FA and RM are listed in Table 1. As seen in Table 1, the FA mainly comprises high contents of SiO_2 and Al_2O_3 (a total content up to 82.46 wt. %) which commonly serve as glass network formers and framework compositions of sintered ceramics [4, 8]. There is a high content of Al_2O_3 (44.63 wt. %) and Fe_2O_3 (31.71 wt. %) in the RM. Otherwise, there are a small amount of alkaline oxides (K_2O, Na_2O) and alkaline earth oxides (CaO, MgO) in the FA and RM, which can decrease the melting point of green bodies [8] and, therefore, promote the sintering process of the samples. Sodium borate was added into the batches of the samples as a sintering aid.

The XRD patterns of the two waste materials are shown in Figure 1. The main crystalline phases of the fly ash are mullite and hydroxy-sodalite, while an amorphous silicate glassy phase is also detected. Compared with the fly ash, the mineral phases of the red mud are identified as cancrinite, hematite and minor titania.

Preparation of the samples

The experimental operation is as follows: firstly 40 wt. % FA and 40 wt. % RM with 20 wt. % borax as the fluxing agent were mixed by ball-milling for 4 h to obtain the homogenous mixtures. Afterwards, green pellets of 30 mm in diameter were formed by uniaxial pressing at 15 MPa. At last, the green bodies were fired at 600 ~ 750 °C using dwell times for 10 ~ 120 min in a muffle furnace, with the heating rate of 5 °C·min^{-1} in an air atmosphere, and then the samples were naturally cooled down to room temperature.

Characterisation

The chemical compositions of the raw materials were determined by X-ray fluorescence spectroscopy of an S8 TIGER. The thermal analysis was taken on by a differential scanning calorimetry (TGA/DSC1) with a heating rate of 10 °C·min^{-1}. The macrostructure observations of the ceramic foams were obtained by digital camera and the microstructure of the samples was observed by a scanning electron microscope (SEM, QUANTA 250 FEG). The bulk density of the porous specimen was calculated as the ratio of the mass and volume based on the Archimedes method. The total porosity was obtained by Equation 1:

$$P\,(\%) = \left(1 - \frac{d_b}{d_p}\right) \times 100\,\% \qquad (1)$$

where d_b represents the bulk density and d_p is the powder density. The water absorption was evaluated by the waterlogged method with deionised water as the liquid medium. The samples with a size of 10 × 10 × × 10 mm^3 were immersed in boiling water for 5 h followed by natural cooling to room temperature.

Table 1. The chemical compositions of the raw materials (wt. %).

Constituents	SiO_2	Al_2O_3	CaO	Fe_2O_3	SO_3	TiO_2	MgO	K_2O	Na_2O	LOI
FA	44.63	37.83	3.88	3.15	1.57	0.97	0.80	0.58	0.52	6.07
RM	2.83	44.63	1.57	31.71	0.97	3.15	0.12	0.15	3.88	10.99

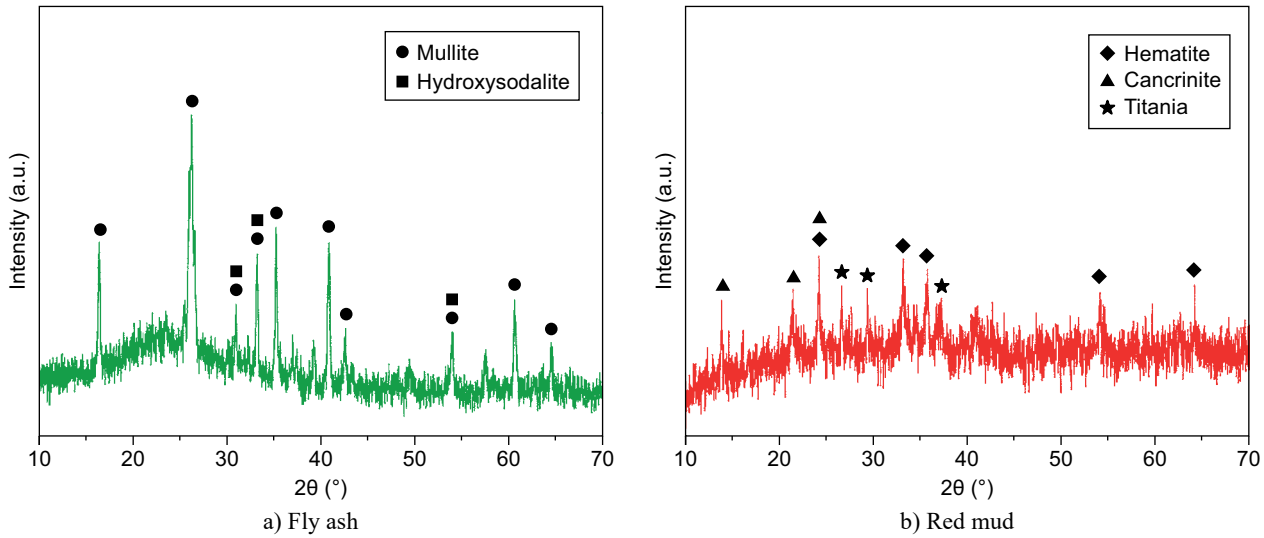

a) Fly ash b) Red mud

Figure 1. The XRD patterns of the fly ash and red mud.

The water absorption was calculated from the dry mass (m_d) and the wet mass (m_s) by Equation 2:

$$W(\%) = \left(\frac{m_s}{m_d} - 1\right) \times 100\ \% \qquad (2)$$

The compressive strength of the samples with the dimension of 10 × 10 × 10 mm^3 was tested by a universal electronic machine (CMT5504) with a cross head speed of 1 mm/min. Each final result is the average from the experiment that was repeated five times.

RESULTS AND DISCUSSION

Effect of the sintering temperature

Figure 2 presents the surface morphology and internal pore structure of the ceramic foams formed at the sintering temperature from 600 °C to 750 °C. The samples show the different volume expansion at the different sintering temperature. From 600 °C to 650 °C, there exists a rapid change in the volume expansion for the sample. With the continuing rising of the sintering temperature, the volume expansion increases slightly. The maximum volume expansion for the sample at a temperature of 675 °C can be realised. However, the volume expansion of the sample diminishes as the temperature is further increased. Similar to the volume change, the porosity and pore diameter increase gradually when the sintering temperature increases from 600 °C to 675 °C. Based on the theory of liquid-phase sintering, the liquid phase starts to appear as the sintering temperature is close to the softening point [12]. Then the sample releases gas and, thus, the formation of gas bubbles can be achieved. The rising temperature leads to a decline in the liquid-phase viscosity and, thus, an increasing in the gas volume under the action of surface tension [13] that accompanies the volume expansion of the sample. At 675 °C, the diameters of the pores become relatively uniform. At this time, the surface tension between the gas and liquid phase achieve a balance so that the pores are very plump and uniform. However, when the gas pressure reaches a high enough level with a further increase in the temperature of 700 ~ 750 °C, the gas can burst out of the surrounding liquid phase and, thus, the connected pores emerge in body.

Figure 3 shows the evolution of the bulk density, porosity, water absorption and compressive strength of the samples with the sintering temperature, respectively. With an increase in the temperature, both the bulk density and compressive strength decrease rapidly, whereas both the porosity and water absorption rise dramatically at the beginning. Then, the change trend becomes slight as the temperature is further raised. When the temperature is up to 675 °C, the extreme value of the entire index can be achieved. With a continuing temperature rise, all the index values show the adverse change tendency due to the appearance of the connected pores in the ceramic foam. Apparently, very close correlations exist between the pore structures and the properties, namely the rising porosity and volume expansion are highly responsible for the declining bulk density and compression strength of the samples. Meanwhile the variation in the water absorption is directly related to the change in the porosity, especially when correlated with the number of opening pores within the sample [4]. It is indicated that the optimal sample presents a result with a bulk density of 358 ± 20 kg·m^{-3}, a porosity of 75.7 ± 2.8 %, a water absorption of 2.71 ± 0.14 % and a compressive strength of 2.38 ± 0.23 MPa at the sintering temperature of 675 °C.

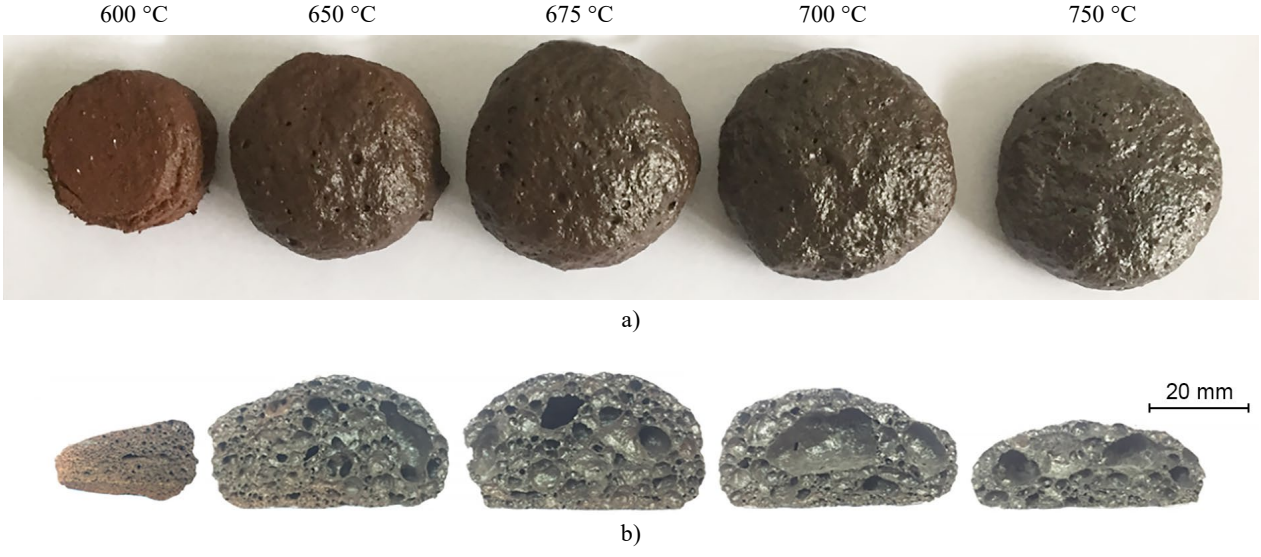

Figure 2. The surface morphology (a) and internal pore structure (b) of the samples at the different sintering temperature.

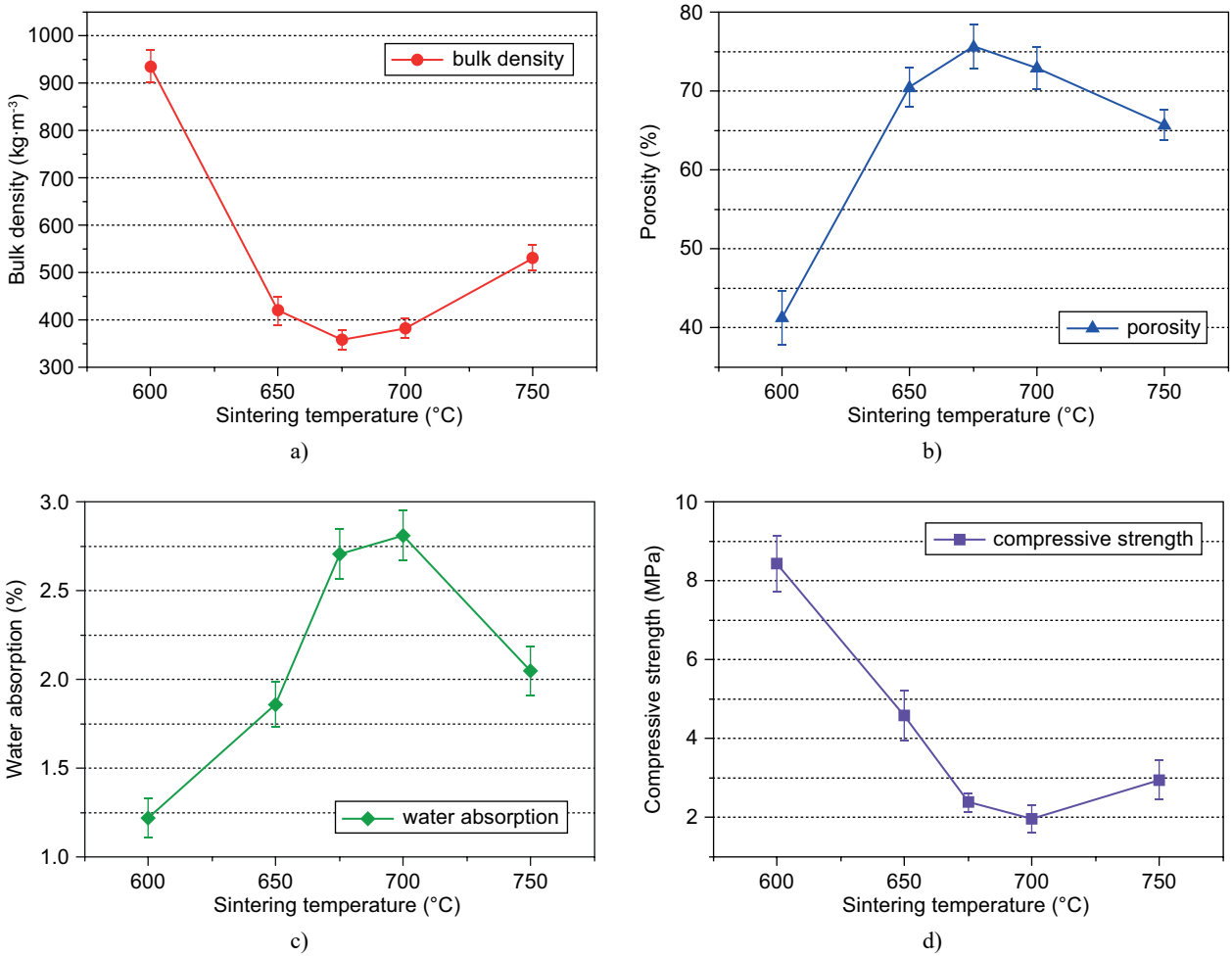

Figure 3. The bulk density (a), porosity (b), water absorption (c) and compressive strength (d) of the samples at the different sintering temperature.

Effect of the holding time

Figure 4 displays the internal pore structure of the samples formed for the different holding times. When the holding time is prolonged from 10 min to 60 min, the volume expansion of the samples increases gradually due to the higher gas generation. From 60 min to 120 min, the change trend is slight, implying it is near the end of the gas release. Meanwhile, the corresponding pore size distribution is shown in Figure 5, the pore diameter enlarges along with the increasing holding time, the curves of the pore size distribution shift to large pores. However, connected pores distinctly appear in the sample with a holding time of 120 min, the pore shape is long, but not round, and, thus, the pore size distribution dramatically widens. This is because the excessive gas expansion with the high-pressure results in the escape of gases so that interconnected pores are achieved in the sintered body.

Figure 6 depicts the effect of the holding time on the bulk density, porosity, water absorption and compressive strength of the porous samples, respectively. As the holding time prolongs from 10 min to 60 min, both the bulk density and compressive strength diminish gradually, while both the porosity and water absorption present an adverse change trend due to the increasing

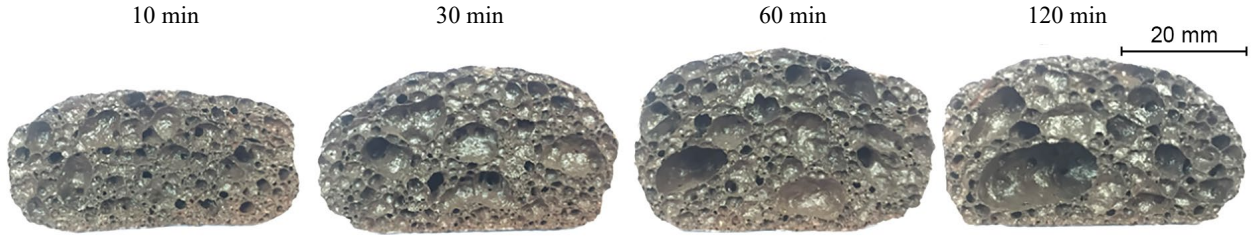

Figure 4. The internal pore structure of the samples formed for the different holding times.

volume expansion of the samples. With the continuing prolonging of the holding time, the change tendency of the bulk density and porosity is not evident, and both the water absorption and compressive strength change slightly, which is consistent in the change trend of the internal pore structure shown in Figure 4. It is indicated that the optimal sample with the holding time of 60 min exhibits a result with a bulk density of 331 ± 10 kg·m^{-3}, a porosity of 83.8 ± 1.8 %, a water absorption of 2.91 ± 0.14 % and a compressive strength of 1.96 ± 0.13 MPa. Based on this result, possible applications of the synthesised porous ceramic involve insulation, gardening and lightweight constructions.

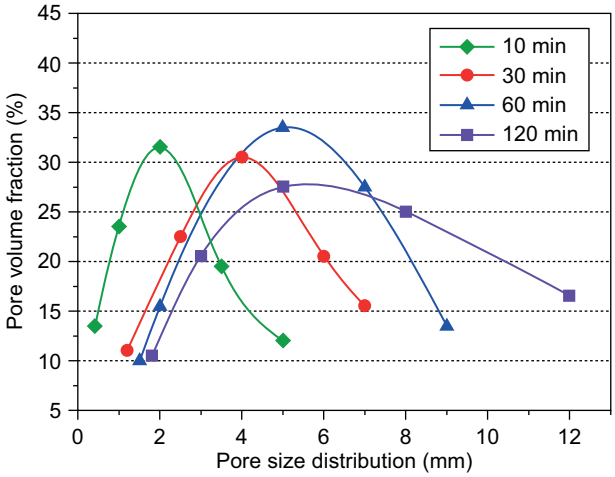

Figure 5. The pore size distribution of the samples with the different holding times.

Self-foaming mechanism

The microstructure of the sample sintered at 675 °C for 60 min is shown in Figure 7. It can be seen that the microstructure is mainly composed of many closed pores with different pore-sizes and pore walls. The diameter of the large pores is about 0.4 ~ 0.8 mm (Figure 7b), the size of the small pores on the walls is 5 ~ 20 μm (Figure 7c), and the pore wall is relatively smooth and dense (Figure 7d). Such a structure should be beneficial to the physical and mechanical properties of porous ceramics. It is reported that the potential sources of gas evolution in the RM and FA mixture that lead to the porous microstructure of the sintered samples may be one or more of the following:

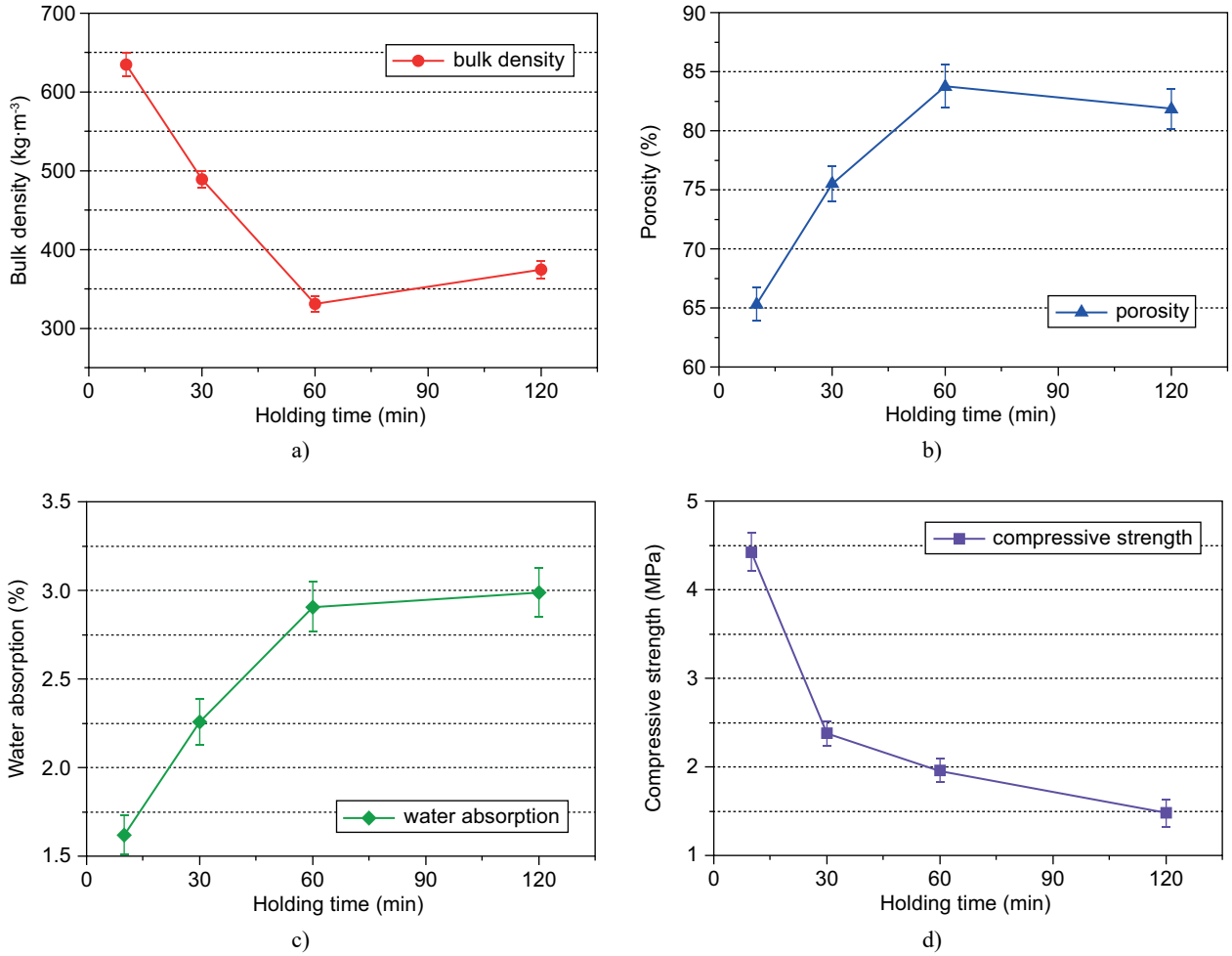

Figure 6. The bulk density (a), porosity (b), water absorption (c) and compressive strength (d) of the samples for the different holding times.

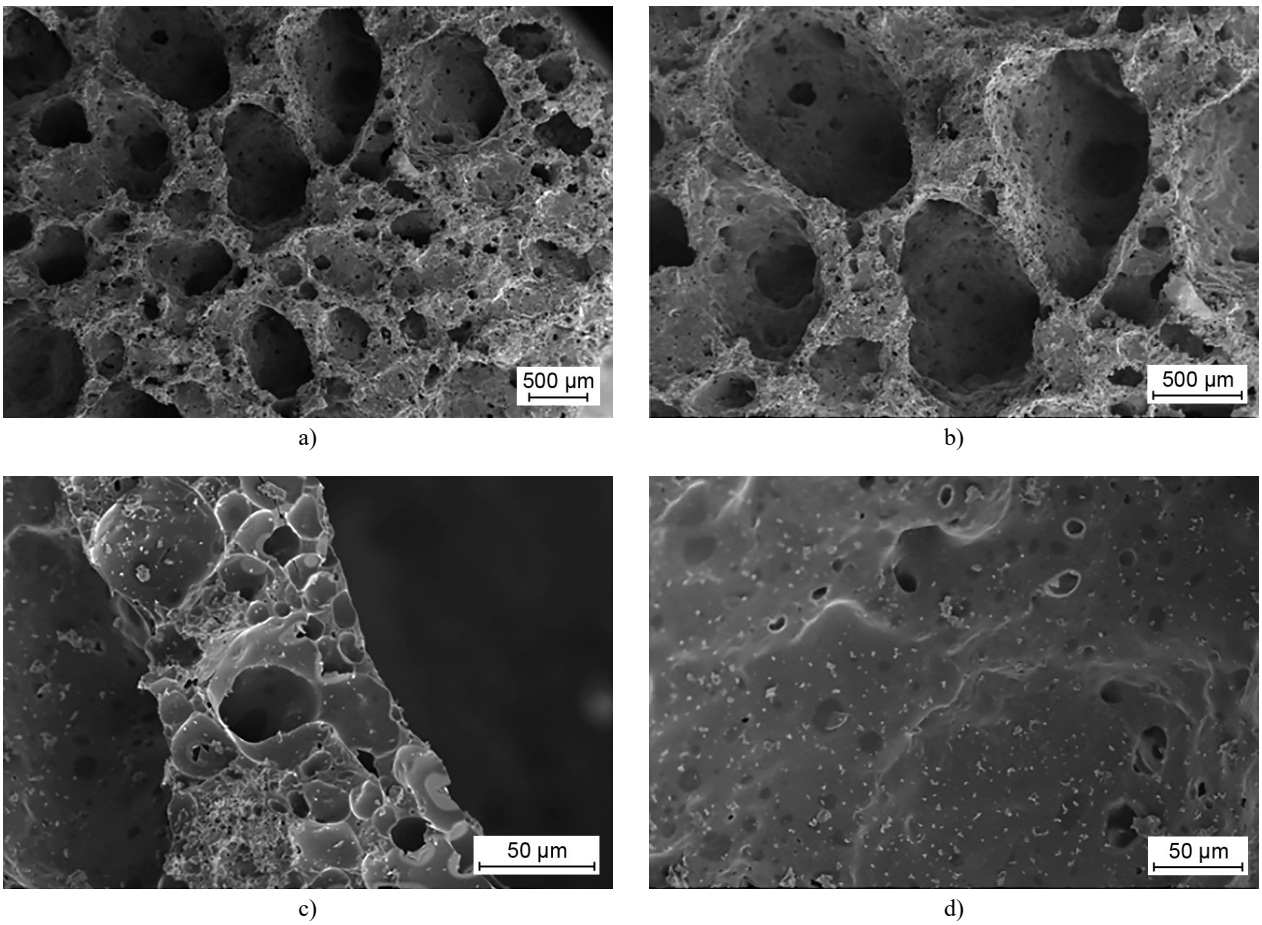

Figure 7. The morphology of the surface (a, b), the cross-section of the pore wall (c) and the surface of the pore wall (d) of the sample sintered at 675 °C for 60 min.

organic matters, calcium carbonate, ferric oxide, hydrated calcium sulphate and entrapped air [3, 5, 14]. In order to address the pore-forming process of the studied mixtures in this study, the DSC-TG (Differential scanning calorimetry-Thermogravimetry) curves of the FA and RM are presented, shown in Figure 8. The DSC curve of the FA reveals two obvious peaks. The early endothermic peak at 158 °C reflects the loss of the free water and the adsorbed water. This is followed by an exothermic peak obtained at 543 °C, which is attributed to the combustion of the organic materials and/or decomposition of the carbonate species in the FA. Accordingly, the TG curve indicates two obvious weight loss processes. A 2.41 % weight loss emerges within the 40 ~ 400 °C range. A rapid weight loss takes place between 500 ~ 650 °C and reaches 2.18 %. It is suggested that such a weight loss is associated with the CO_2 emission arising from the organic materials and carbonates. With respect to the RM, one endothermic peak and two exothermic peaks are observed at 181 °C, 296 °C and 736 °C, respectively, for the DSC curve, which are relevant with the corresponding mass loss in the TG curve. The peaks at 181 °C and 296 °C are connected with the loss of the physically adsorbed water and the burnout of the organic materials, while the peak at 736 °C is linked to the decomposition of the calcite in the RM.

For a homogenous green body, when the sintering temperature comes up to the softening point, the green body initiates melting and then the generation of a certain amount of liquid phase can be realised under the action of the fluxing agent which can lower the softening temperature point and make the composition to be close to the formation range of the glassy phase [12, 15-17]. At this time, the gas, which was released according to the DSC-TG curves, occurs and dissolves in the melt to diffuse into bubbles and makes them expand. The bubble radius r is governed by the temperature according to Equation 3 [18]:

$$r\,(T,\,t) = \beta\,\sqrt{D\,(T,\,t)\,t} \tag{3}$$

Here, β is a dimensionless empirical constant, T is the foaming temperature and $D(T,\,t)$ is the effective diffusion coefficient.

$$D\,(T,\,t) = \frac{k_B T}{6\pi\eta\,(T,\,t)\,r_g} \tag{4}$$

where k_B is Boltzmann's constant, and r_g is the radius of the gas molecules. With the further growth, the bubbles

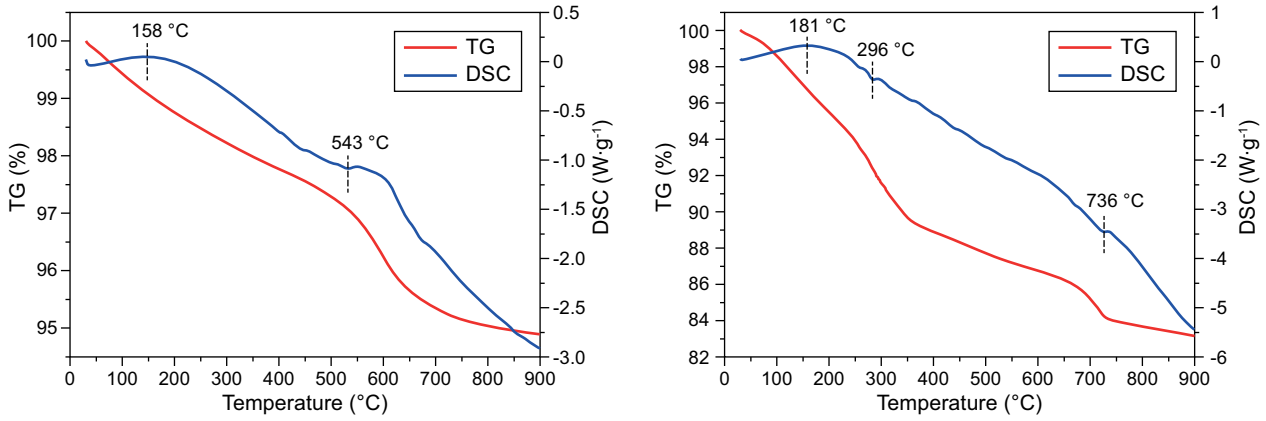

a) Fly ash

b) Red mud

Figure 8. The DSC-TG curves of the studied FA and RM.

approach each other and start to touch until equilibrium is reached during the insulation stage [19], the diameters of the pores become uniform and the pore walls become thin [20]. The insulation process can bring the surface tension of the liquid phase (γ_l) and the gas pressure (P_g) into balance, as illustrated in Figure 9. In fact, γ_l is just higher than P_g at the appropriate temperature [21, 22], the ideal pore structure with plump pores and a smooth pore wall can be obtained. As the temperature decreases, the surface energy and viscosity decrease simultaneously, the uniform pores are solidified in the body stably [23, 24], thus forming a typical porous foam. However, when the surface tension between the gas and liquid phase reaches a certain level with the rising temperature and/or holding time, the gas will be able to escape to form connected pores in the body.

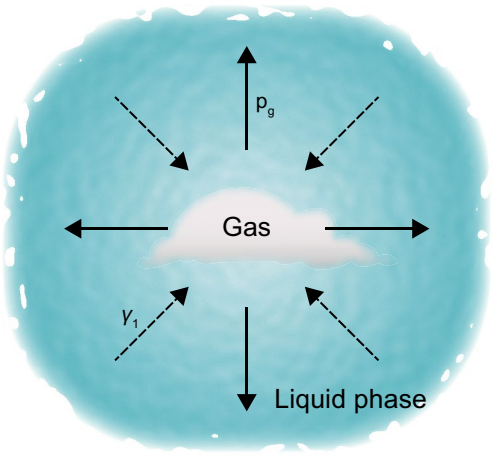

p_g – Gas pressure, γ_1 – Surface tension

Figure 9. An illustration of the match between the liquid phase and the gas emission of the sample.

CONCLUSIONS

A self-foaming ceramic foam was obtained that was derived from fly ash (FA) and red mud (RM). With the rising sintering temperature, both the bulk density and compressive strength first decreased rapidly and then increased, whereas both the porosity and water absorption increased first and then decreased. There was a similar regular variation trend of such properties with the different holding times. With the holding time being prolonged, the porosity increased while the bulk density decreased. The compressive strength decreased while the water absorption increased with an increase in the porosity. When sintered at 675 °C for 60 min, the ceramic foam exhibited promising properties with a bulk density of 331 ± 10 kg·m^{-3}, a porosity of 83.8 ± 1.8 %, a water absorption of 2.91 ± 0.14 % and a compressive strength of 1.96 ± 0.13 MPa, which will have good potential applications in the insulation, gardening and lightweight construction industries. It was found that the porous ceramics performed a self-foaming process in the course of the sintering, probably arising from the combustion of the organic materials and/or decomposition of the carbonates in the studied FA and RM. This study indicates that the preparation and application of porous ceramics based on RM and FA may be an effective solution for solid waste resource utilisation and for the minimisation of natural resources.

Acknowledgements

This work was supported by the Shandong Provincial Natural Science Foundation of China (ZR2018LE004), the Major Basic Research Program of the Shandong Provincial Natural Science Foundation of China (ZR2018ZC0741), the National Key Research and Development Program of China (2017YFC0703100), the National Key Research and Development Program

of China (2016YFB0303505), the National Natural Science Foundation of China (51632003), the Taishan Scholars Program and the Case-by-Case Project for Top Outstanding Talents of Jinan.

REFERENCES

1. Chen H., Wang S., Tang C. (2010): Reuse of incineration fly ashes and reaction ashes for manufacturing lightweight aggregate. *Construction and Building Materials, 24*(1), 46-55. doi: 10.1016/j.conbuildmat.2009.08.008
2. Li J., Zhuang X., Monfort E., Querol X., Llaudis A. S., Font O., Izquierdo M. (2018): Utilization of coal fly ash from a Chinese power plant for manufacturing highly insulating foam glass: Implications of physical, mechanical properties and environmental features. *Construction and Building Materials, 175*, 64-76. doi: 10.1016/j.conbuildmat.2018.04.158
3. Guo Y., Zhang Y., Huang H., Meng K., Hu K., Hu P., Meng X. (2014): Novel glass ceramic foams materials based on red mud. *Ceramics International, 40*(5), 6677-6683. doi: 10.1016/j.ceramint.2013.11.128
4. Hou L., Liu T., Lu A. (2017): Red mud and fly ash-based ceramic foams using starch and manganese dioxide as foaming agent. *Transactions of Nonferrous Metals Society of China, 27*(3), 591-598. doi: 10.1016/s1003-6326(17)60066-9
5. González-Corrochano B., Alonso-Azcárate J., Rodas M. (2009): Characterization of lightweight aggregates manufactured from washing aggregate sludge and fly ash. *Resources, Conservation and Recycling, 53*(10), 571-581. doi: 10.1016/j.resconrec.2009.04.008
6. Chen X., Lu A., Qu G. (2013): Preparation and characterization of foam ceramics from red mud and fly ash using sodium silicate as foaming agent. *Ceramics International, 39*(2), 1923-1929. doi: 10.1016/j.ceramint.2012.08.042
7. Liu T., Tang Y., Li Z., Wu T., Lu A. (2016): Red mud and fly ash incorporation for lightweight foamed ceramics using lead-zinc mine tailings as foaming agent. *Materials Letters, 183*, 362-364. doi: 10.1016/j.matlet.2016.07.041
8. Liu T., Lin C., Liu J., Han L., Gui H., Li C., Lu A. (2018): Phase evolution, pore morphology and microstructure of glass ceramic foams derived from tailings wastes. *Ceramics International*, *44*(12), 14393-14400. doi: 10.1016/j.ceramint.2018.05.049
9. Chen B., Wang K., Chen X., Lu A. (2012): Study of foam glass with high content of fly ash using calcium carbonate as foaming agent. *Materials Letters, 79*, 263-265. doi: 10.1016/j.matlet.2012.04.052
10. Chen B., Luo Z., Lu A. (2011): Preparation of sintered foam glass with high fly ash content. *Materials Letters, 65*(23-24), 3555-3558. doi: 10.1016/j.matlet.2011.07.042
11. Luo Y., Zheng S., Ma S., Liu C., Wang X. (2018): Preparation of sintered foamed ceramics derived entirely from coal fly ash. *Construction and Building Materials, 163*, 529-538. doi: 10.1016/j.conbuildmat.2017.12.102
12. Hasheminia S., Nemati A., Eftekhari Yekta B., Alizadeh P. (2012): Preparation and characterisation of diopside-based glass-ceramic foams. *Ceramics International, 38*(3), 2005-2010. doi: 10.1016/j.ceramint.2011.10.035
13. Dondi M., Cappelletti P., D'Amore M., Gennaro R., Graziano S. F., Langella A., Zanelli C. (2016): Lightweight aggregates from waste materials: Reappraisal of expansion behavior and prediction schemes for bloating. *Construction and Building Materials, 127*, 394-409. doi: 10.1016/j.conbuildmat.2016.09.111
14. Wang H., Chen Z., Ji R., Liu L., Wang X. (2018): Integrated utilization of high alumina fly ash for synthesis of foam glass ceramic. *Ceramics International, 44*(12), 13681-13688. doi: 10.1016/j.ceramint.2018.04.207
15. Soltan A. M. M., Kahl W., Abd El-Raoof F., Abdel-Hamid El-Kaliouby B., Abdel-Kader Serry M., Abdel-Kader N. A. (2016): Lightweight aggregates from mixtures of granite wastes with clay. *Journal of Cleaner Production, 117*, 139-149. doi: 10.1016/j.jclepro.2016.01.017
16. Souza M. T., Maia B. G. O., Teixeira L. B., Oliveira K. G., Teixeira A. H. B., Novaes Oliveira A. P. (2017): Glass foams produced from glass bottles and eggshell wastes. *Process Safety and Environmental Protection, 111*, 60-64. doi: 10.1016/j.psep.2017.06.011
17. Liu M., Xu G., Li G. (2017): Effect of the ratio of components on the characteristics of lightweight aggregate made from sewage sludge and river sediment. *Process Safety and Environmental Protection, 105*, 109-116. doi: 10.1016/j.psep.2016.10.018
18. Nagrath, S., Jansen, K. E., Lahey, R. T. (2005): Computation of incompressible bubble dynamics with a stabilized finite element level set method. *Computer Methods in Applied Mechanics and Engineering, 194*(42), 4565-4587. doi: 10.1016/j.cma.2004.11.012
19. Bai, J., Yang, X., Xu, S., Jing, W., & Yang, J. (2014): Preparation of foam glass from waste glass and fly ash. *Materials Letters, 136*, 52-54. doi: 10.1016/j.matlet.2014.07.028
20. Jiang C., Huang S., Li G., Zhang X., Cheng X. (2018): Formation of closed-pore foam ceramic from granite scraps. *Ceramics International, 44*(3), 3469-3471. doi: 10.1016/j.ceramint.2017.10.180
21. Zhang Q., He F., Shu H., Qiao Y., Mei S., Jin M., Xie J. (2016): Preparation of high strength glass ceramic foams from waste cathode ray tube and germanium tailings. *Construction and Building Materials, 111*, 105-110. doi: 10.1016/j.conbuildmat.2016.01.036
22. Zhai C., Li Z., Zhu Y., Zhang J., Wang X., Zhao L., Wang P. (2014): Effects of Sb_2O_3 on the Mechanical Properties of the Borosilicate Foam Glasses Sintered at Low Temperature. *Advances in Materials Science and Engineering, 2014*, 1-6. doi: 10.1155/2014/703194
23. Bernhardt M., Justnes H., Tellesbø H., Wiik K. (2014): The effect of additives on the properties of lightweight aggregates produced from clay. *Cement and Concrete Composites, 53*, 233-238. doi: 10.1016/j.cemconcomp.2014.07.005
24. Moreno-Maroto J. M., González-Corrochano B., Alonso-Azcárate J., Rodríguez L., Acosta A. (2017): Manufacturing of lightweight aggregates with carbon fiber and mineral wastes. *Cement and Concrete Composites, 83*, 335-348. doi: 10.1016/j.cemconcomp.2017.08.001